Study On Acoustic Characteristics Of Internal Leakage Of Micro-start Spring Safety Valve

Shuxun Li[1,2], Xuedong Zhang[1,2*], Yunxin Kang[3], Jianjun Hou[1,2], and Jingwei Liu[1,2]

[1] School of Petrochemical Engineering, Lanzhou University of Technology, Lanzhou 730050, China
[2] Mechanical industry pump and special valve Engineering Research Center, Lanzhou 730050, China
[3] 210 Institute of the Sixth Academy of CASIC, Xi'an 710000, China
[*] Corresponding author. E-mail: zhangxuedong3569@163.com

Received: September 19, 2022; Accepted: March. 03, 2023

To investigate the noise radiation in the leakage of the safety valve. The acoustic fluid-solid coupling simulation analysis of the leakage process of the safety valve is used to study the flow field when the safety valve is leaking. The sound source characteristics of different inlet pressures and different leakage holes when the internal leakage of the safety valve occurs are analyzed, and the noise source is analyzed in combination with the flow field simulation. The results show that when the internal leakage of the safety valve occurs, the noise is mainly dominated by the quadrupole sound source caused by the jet, accompanied by the dipole sound source. At the same time, the noise sound pressure level is positively correlated with the working medium pressure of the safety valve and is quadratically correlated with the inner leakage hole.

Keywords: Safety valve; Internal leakage noise; Numerical simulation; Acoustic characteristics; Acoustic-fluid-solid coupling

http://dx.doi.org/10.6180/jase.202312_26(12).0009

1. Introduction

The safety valve is an important part of the pipeline system, which plays an important role in ensuring pipeline safety. However, due to a series of practical operations such as manufacturing, installation, use and later maintenance, the sealing surface of the safety valve may be damaged, which causes the valve leakage, and affect the pipeline system safety and lead to valve leakage affecting the pipeline system safety [1]. And the noise is harmful to us, not only to the body but also to the hearing [2–5].

Valve acoustic research mainly focuses on acoustic characteristics, internal leakage location, and acoustic emission fault detection. Javad Taghinia et al. [6] use the large eddy simulation method to investigate the flow structure in an HPH valve. Then based on the Large Eddy Simulation (LES) model, the Discrete Phase Model (DPM) model, and the Ffowcs Williams-Hawkings (FW-H) model, Chen et al.[7] take a further study that proposes and verifies a fluid-solid-acoustic multi-physics coupling DPM-LES model, which can be used to study the flow field dynamic and acoustic characteristics of the gas-liquid twin-fluid. Ren et al.[8] obtain the super/transcritical water jet characteristics by using large eddy simulations (LES). Li et al.[9] developed a 3-D model to investigate the flow field and acoustic properties of the two-stream jets. Liao [10] studied the turbulent flow and aerodynamic noise of a half-cylinder on a flat plate by using the higher-order cell-centered finite difference method (CCFDM) delayed separation vortex simulation (DDES) and large vortex simulation (LES), and the results showed that the LES method has better results in solving the delayed separation vortex simulation problem. S.A. Hambric et al. [11] computed the structure- and fluid-borne vibroacoustic power spectra induced by turbulent fluid flow over the walls of a continuous 90 piping elbow

Then, Zhang et al. [12] investigated the structural vibration and fluid-borne noise induced by turbulent flow through a 90° piping elbow using the hybrid LES/Lighthill's acoustic analogy method. The turbulence numerical simulation, aero-acoustic simulation, and acoustic boundary element method (BEM) are used to simulate the aero-dynamic noise of turbocharger compressors in literature [13–16]. Zhang et al. [17] study the time-frequency signal of pipe leakage acoustic waves by using the method of "acoustic-pipe and acoustic-pressure" multi-physical field coupling. The results show that the acoustic wave propagates from the leakage hole, and the amplitude decreases rapidly. Liu et al. [18] establish a computational aero-acoustic (CAA) model of the internal and external field noise of a marine pump and obtain the spectrum characteristics of internal and external field noise by using the coupled acoustic vibration method. The results show that the radiation noise induced by the fluid excitation is higher than that induced by the dipole excitations. Qian et al. analyze the acoustic response of various thick perforated plates by using the Finite element method (FEM) and propose a linear correction formula of maximum TL. Wang et al.[19] propose a novel FWRV (four-way reversing valve), which can be used to reduce friction-induced vibration and improve fluency. Li et al.[20] proposed a numerical simulation method for the aerodynamic noise of safety valves that comprehensively considers quadrupoles and dipoles. Test results show that the simulation method can achieve an accuracy of less than 10% under different working conditions.

In summary, the current research has carried out theoretical research on the sound source of the valve and pipeline leakage, and proposed a variety of leakage analysis methods based on classical acoustic theory. At the same time, previous studies have shown that the LES turbulence model has a very high advantage in studying the problem of medium leakage. The purpose of this paper is to study the law between the working pressure and leakage parameters of the safety valve and the characteristics of the leakage sound source. The LES turbulence model is used to analyze the internal flow characteristics of the safety valve under the internal leakage condition. Through the analysis of the flow information, the noise source of the internal leakage of the safety valve is obtained. Based on the fluid dynamics and Lighthill acoustic analogy theory, the internal leakage of the safety valve is numerically simulated and analyzed by considering the acoustic fluid-solid coupling of the dipole and the quadrupole. The distribution and mutual law of the internal leakage sound source characteristics of the safety valve under different pressures, different apertures, and different internal leakage forms are calculated. According to the quantitative law of the internal leakage of the safety valve and its corresponding acoustic characteristics under different working conditions, a mathematical model characterizing the internal leakage of the safety valve and the sound pressure level is established.

2. The research object

Comprehensively considering the test requirements and the characteristics of the internal leakage sound source, the micro-start spring load safety valve is selected as the research object. Its main structure is shown in Fig. 1, and the relevant key parameters are shown in Table 1.

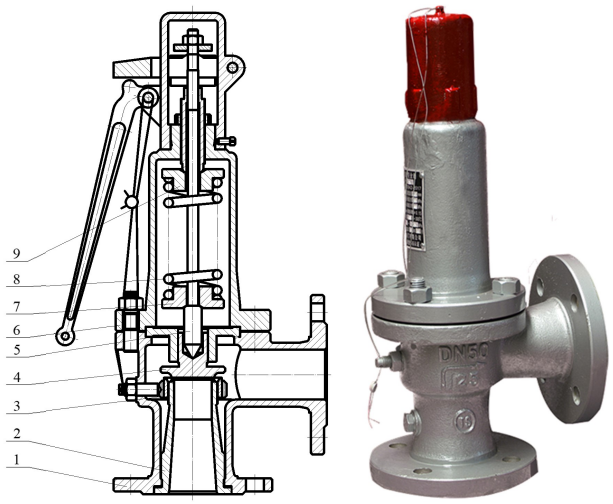

Fig. 1. The 50A47H-16C spring load safety valve. 1 valve body; 2 valve seats; 3 regulating circles; 4 valves; 5 stems; 6 valve covers; 7 lower spring seats; 8 springs; 9 upper spring seat.

Table 1. Main technical parameters table of safety valve.

Name	Parameter
PN	16
DN	50
Opening height /mm	2 mm
Setting pressure /MPa	0.7MPa
Emission pressure /MPa	$\leq$ 0.77MPa
return pressure /MPa	$\geq$ 0.60MPa
Design temperature /°C	$\leq$ 350°C

3. Theoretical study on valve aerodynamic noise

3.1. RNG $k-\varepsilon$ model

The flow equations used in the paper are written as:

$$\frac{\partial \rho}{\partial t} + \nabla \cdot (\rho U) = 0 \tag{1}$$

$$\frac{\partial \rho U}{\partial t} + \nabla \cdot (\rho U \otimes U) - \nabla \cdot \left(\mu_{cff} \nabla U\right) = \nabla \cdot p' + \nabla \cdot \left(\mu_{df} \nabla U\right)^{\top} + B \tag{2}$$

where

$$\mu_{\partial f} = \mu + \mu_t \tag{3}$$

$$p' = p + \frac{2}{3}\rho k \tag{4}$$

where B is the body force,

ρ is the density,

U is the velocity,

p' is the fixed pressure,

μ_{sff} is the effective viscosity,

μ_t is the dynamic viscosity,

μ is the molecular viscosity.

The equation for the turbulent kinetic energy k can be obtained by modeling the terms of production, diffusion, and dissipation as follows:

$$\frac{\partial(\rho k)}{\partial t} + \nabla \cdot (\rho U k) = \nabla \cdot \left[\left(\mu + \frac{\mu_t}{\sigma_k}\right) \nabla k\right] + P_k + \rho\varepsilon \tag{5}$$

where σ_k is the turbulent Prandtl number,

ε is the dissipation rate of turbulent kinetic energy,

P_k is the output project of turbulent shear flows,

the dynamic eddy viscosity is then obtained by dimensional considerations:

$$\mu_t = C_\mu \rho \frac{k^2}{\varepsilon} \tag{6}$$

where

C_μ is the constant of the RNG k- ε model.

The closure of the model is obtained by using the equation of the turbulent dissipation rate ε. The turbulent dissipation rate ε c an be written as:

$$\frac{\partial(\rho\varepsilon)}{\partial t} + \nabla \cdot (\rho U \varepsilon) = \nabla \cdot \left[\left(\mu + \frac{\mu_t}{\sigma_{sRNG}}\right) \nabla \varepsilon\right] + \frac{\varepsilon}{k}\left(C^*_{s1RVG} P_k - C_{s2RVG} \rho\varepsilon\right) \tag{7}$$

where

$$C^*{}_{\varepsilon 1RNG} = C_{\varepsilon 1RNG} - f_\eta \tag{8}$$

$$f_\eta = \frac{\eta\left(1 - \frac{\eta}{\eta_0}\right)}{(1 + \beta_{RNG}\eta^3)} \tag{9}$$

$$\eta = \sqrt{\frac{P_k}{\rho C_{\mu RNG}\varepsilon}} \tag{10}$$

where $\sigma_{\varepsilon RAG}$ is the dissipation Prandtl number.

The empirical coefficients are given as $C_{\mu RNG} = 0.0845, C_{\varepsilon IRNG} = 1.42, C_{\varepsilon 2RNG} = 1.68$, $\eta_0 = 4.377$, and $\beta_{RNG} = 0.012$.

3.2. LES numerical methods

Large eddy simulations can solve the problem of three-dimensional transient turbulence, which is composed of eddies of different scales. The basic idea of large eddy simulation is to decompose the instantaneous pulsation in turbulent flow into the solvable scale and sub-lattice scale by filtering. The large-scale quantities are solved directly, and the small-scale quantities are simulated with the subgrid model (SGS).

Filtering N-S equation using discrete volume equation:

$$\frac{\partial \overline{u_i}}{\partial t} + \frac{\partial \overline{u_i u_j}}{\partial \overline{x_j}} = -\frac{1}{\rho}\frac{\partial \bar{p}}{\partial x_i} + v\frac{\partial^2 \overline{x_i}}{\partial x_j \partial x_j} + \frac{\partial \overline{\tau_{ij}}}{\partial x_j} \tag{11}$$

The subgrid stress:

$$\overline{\tau_{ij}} = \left(\overline{u_i u_j} - \overline{u_i u_j}\right) \tag{12}$$

To close the system of equations, according to Smagorinsky's basic SGS model, it is assumed that the SGS Reynolds stress has the following form:

$$\tau_{ij} = -2v_t \overline{s_{ij}} + \frac{1}{3}\tau_{kk}\delta_{ij} \tag{13}$$

where

δ_{ij} is the unit tensor,

v_t is the Subgrid turbulent viscosity coefficient,

$\overline{s_{\text{ij}}}$ is the component of the strain tensor at scale.

$$\overline{s_{ij}} = \frac{1}{2}\left(\frac{\partial \overline{u_i}}{\partial x_j} + \frac{\partial \overline{u_j}}{\partial x_i}\right) \tag{14}$$

3.3. Acoustic calculation

Combining with the fluid equation, Lighthill established the mathematical model of the physical source of flow sound and found a similar correlation between the sound field and the flow field. The Lette Hill equation is derived from the most basic N-S equation to further solve the problem of fluid noise. Curle extends Lighthill's theory and clearly explains the three aerodynamic sound sources of moving objects. Curle's work is further developed, considering the influence of all solid boundaries of Ffowcs Williams and Hawkings in any motion. The generalized FW-H equation is obtained by using the generalized function method. The detailed derivation of the formula is as follows.

Lighthill's basic equations, including the continuity equation of fluid mass conservation in the volume unit and the particle motion equation in the fluid reference element, are shown in Equations 1 and 2.

$$\frac{\partial \rho}{\partial t} + \frac{\partial \rho u_j}{\partial x_j} = 0 \tag{15}$$

$$\rho\frac{\partial u_i}{\partial t}+\rho u_j\frac{\partial u_j}{\partial x_j}=-\frac{\partial p_{ij}}{\partial x_j} \tag{16}$$

Multiplying 15 with u_i and adding 16 to obtain the momentum equation

$$\rho\frac{\partial u_i}{\partial t}+\rho u_j\frac{\partial\left(u_iu_j\right)}{\partial x_j}=-\frac{\partial p_{ij}}{\partial x_j} \tag{17}$$

Introducing the Heaviside function

$$H(f)=\begin{cases}1 & f(x,y)>0\\ 0 & f(x,y)<0\end{cases} \tag{18}$$

When $f(x,t)=0$ is the governing surface equation of the moving boundary, $f(x,t)<0$ represents the space domain of the fluid without perturbation.

By introducing the flow parameter equation of the generalized Heaviside function,

$$\begin{cases}\bar{\rho}=\rho' H(f)+\rho_0\\ \bar{u}_i=u_iH(f)\\ \bar{p}_{ij}=p_{ij}H(f)-p_0\delta_{ij}\end{cases} \tag{19}$$

Derivative of Heaviside function

$$\begin{aligned}\frac{\partial H}{\partial t}&=\frac{\partial H}{\partial f}\frac{\partial f}{\partial t}\\ \frac{\partial H}{\partial x_i}&=\frac{\partial H}{\partial f}\frac{\partial f}{\partial x_i}\end{aligned} \tag{20}$$

The generalized flow parameters are brought into the continuity equation to obtain the generalized continuity equation

$$\frac{\partial}{\partial t}\left[\rho' H(f)\right]+\frac{\partial}{\partial x_i}\left[\rho' H(f)\right]=\rho_0 v_i\frac{\partial f}{\partial x_i}\delta(f) \tag{21}$$

Generalized momentum equation obtained by substituting generalized flow parameter into the momentum equation

$$\frac{\partial}{\partial t}\left[\rho u_iH(f)\right]+\frac{\partial}{\partial x_i}\left[\left(\rho u_iu_j+p_{ij}\right)H(f)\right]=p_{ij}\frac{\partial f}{\partial x_i}\delta(f) \tag{22}$$

The generalized continuous equation is derived for t. The momentum equation takes the scatter, and then both sides of the equation are subtracted by $c_0^2\left\{\partial^2\left[\rho' H(f)\right]/\partial x_i^2\right\}$. Considering $p'=c_0^2\rho'$, we can get

$$\begin{aligned}&\frac{1}{c_0^2}\frac{\partial^2 p'}{\partial t^2}-\nabla^2 p'=\frac{\partial}{\partial t}\left[\rho_0u_n\delta(f)\right]-\\ &\frac{\partial}{\partial x_i}\left[P_{ij}n_j\delta(f)\right]+\frac{\partial^2}{\partial x_ix_j}\left[H(f)T_{ij}\right]\end{aligned} \tag{23}$$

In this paper, the computational domain is $f(x,y)>0, H(f)=1$, thus

$$\frac{1}{c_0^2}\frac{\partial^2 p'}{\partial t^2}-\nabla^2 p'=\frac{\partial}{\partial t}\left[\rho_0u_n\delta(f)\right]-\frac{\partial}{\partial x_i}\left[P_{ij}n_j\delta(f)\right]+\frac{\partial^2}{\partial x_ix_j}T_{ij} \tag{24}$$

In Eq. 10, the first term on the right side is a monopole, the second term is a dipole, and the third term is a quadrupole. Among them, the monopole generally refers to the unstable state at low velocities and is usually not considered. Dipole occurs in the airflow and solid boundary coupling caused by pressure pulsation radiation out of the noise. The quadrupole sound source generates high-speed flow, when the Mach number is low, then do not need to consider the quadrupole sound source. In the safety valve internal leakage noise applications, the internal leakage noise belongs to the second-term dipole sound source and the third-term quadrupole combination.

4. Flow and noise analysis of safety valve

4.1. Method

As shown in Fig. 2, the noise analysis process is that the flow channel model is obtained by reverse modeling, and then the RNG $k-\varepsilon$ turbulence model is used to calculate the steady flow field. Based on the convergence result of the steady flow field, the transient flow field is calculated by a large eddy simulation turbulence model by using the same boundary conditions. Finally, the .cgsn file of pressure information is derived as a dipole sound source and the .cgsn file of velocity information is derived as a quadrupole sound source to calculate the acoustic response. Among them, acoustic response 1 is calculated by dipole source as acoustic excitation source, acoustic response 2 is calculated by quadrupole source as acoustic excitation source, and acoustic response 3 is calculated by dipole and quadrupole as acoustic excitation source at the same time.

4.2. Fluid domain grid model and flow field boundary conditions

The inner flow channel model of the safety valve is shown in Fig. 3, and on the left side is the grid zoom at the leak hole. A round hole of diameter d=1mm is used instead of leak holes of different shapes. The unstructured grids are used for adaptive division, and the grids in the internal leakage region and the turbulent region after the internal leakage region are encrypted to ensure calculation accuracy. The wall is set as a smooth wall, with no-slip boundary condition, the standard wall function is used in the near wall area, and the influence of gravity acceleration is considered. The second-order upwind discretization scheme is adopted for the control equations such as velocity, turbulent kinetic energy dissipation rate, and turbulent kinetic energy, and the central difference scheme is adopted for the pressure term. Pressure boundary conditions are adopted for both import and export. And verify the grid independence. Based on calculating the steady-state convergence

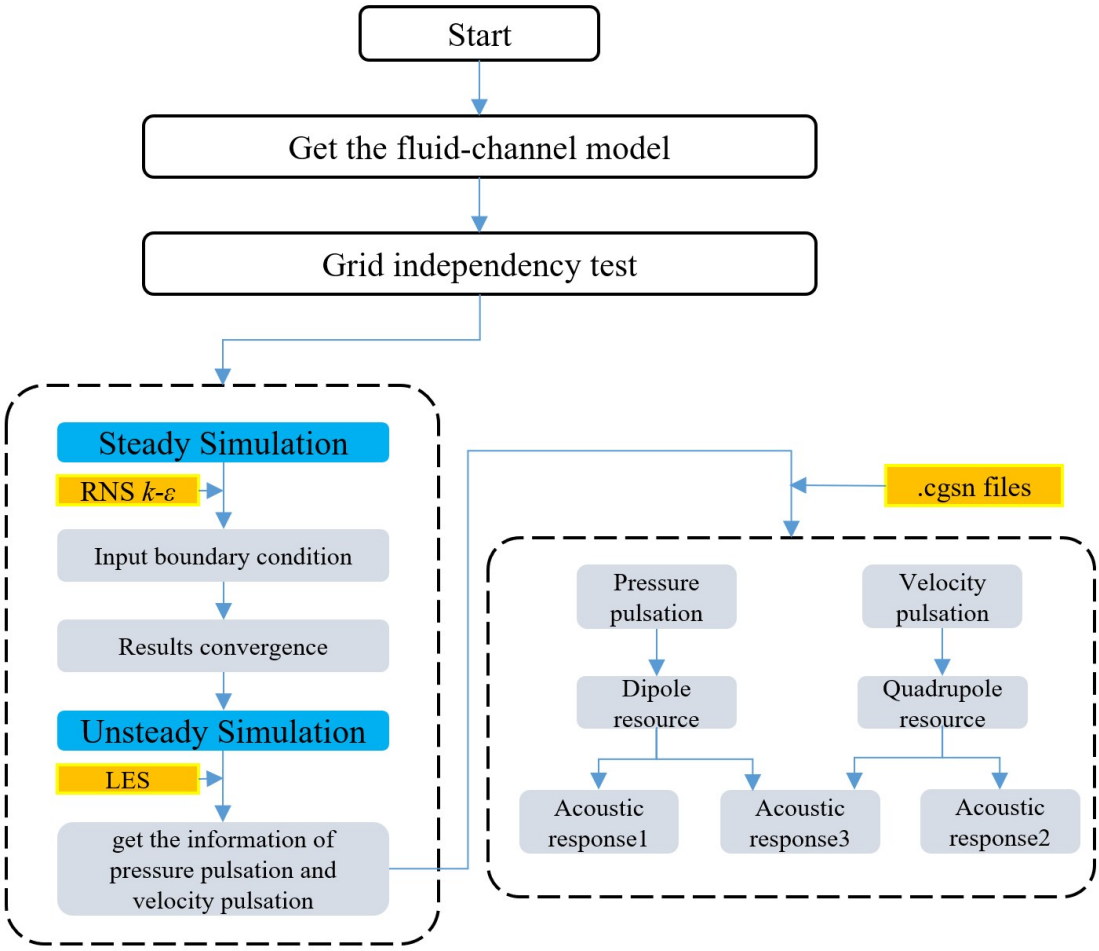

Fig. 2. Noise analysis flow chart.

of the flow field based on the RNG $k-\varepsilon$ turbulence model, the transient simulation of the convection field based on the LES turbulence model is carried out. The transient flow field streamline is shown in Fig. 4.

It can be seen from Fig. 4 that the fluid velocity in the internal flow field of the safety valve has no obvious change. In the small area on the left side of the leak hole, the fluid velocity begins to change; inside the leak hole, the gas velocity changes sharply; on the right side of the leak hole, the fluid velocity drops rapidly and forms a vortex. It can be seen from the pressure program that the pressure ratio before and after throttling is about 1.93. When the medium flows through the leakage hole, the fluid will expand rapidly after compression, and this process will interact with the inner wall surface of the structure, resulting in a strong pulsating pressure, thus forming a dipole sound source. At the same time, due to the throttling effect, the jet effect is formed in the region behind the gap, and the velocity gradient increases to form a quadrupole sound source. As shown in Figure 4, the speed of the throttle reaches 212.1 m/s. At this point, the leakage hole is mainly a quadrupole sound source. with dipoles

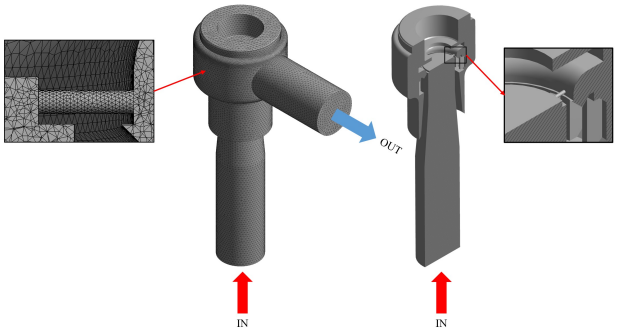

Fig. 3. Grid diagram of the flow passage in the safety valve.

Taking the case, in which the inlet pressure of 0.13 MPa and outlet pressure of 0.1 MPa, as examples, the flow velocity at the internal leakage hole is monitored and the Mach

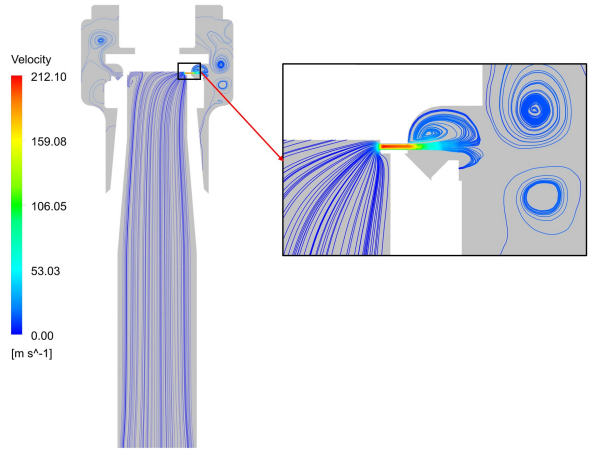

Fig. 4. Internal flow chart of safety valve.

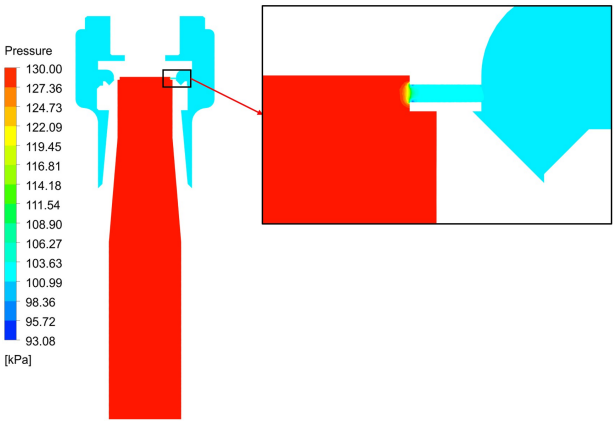

Fig. 5. Flow pressure cloud diagram of safety valve.

number is calculated:

$$\mathrm{Ma} = \frac{v}{c_0} \tag{25}$$

where Ma is the Mach number, v is the medium velocity, and c is the local sound velocity; the calculated Ma is 0.62 0.3, belonging to a subsonic flow, dominated by quadrupoles, and dipoles and quadrupoles jointly contribute sound source information. The sound source information obtained by Fluent is combined with LMS Virtual. Lab for acoustic fluid-solid coupling analysis. The sound source information of the fluid grid node is loaded into the acoustic boundary element mesh as the sound field excitation to map the information. The sound source information is shown in Figure 6 and Figure 7.

The node information of the flow field grid is mapped to the boundary element grid by the non-energy loss theory algorithm. The time domain information of the dipole sound source is converted by the FFT frequency domain, and the information of the quadrupole sound source is analyzed by

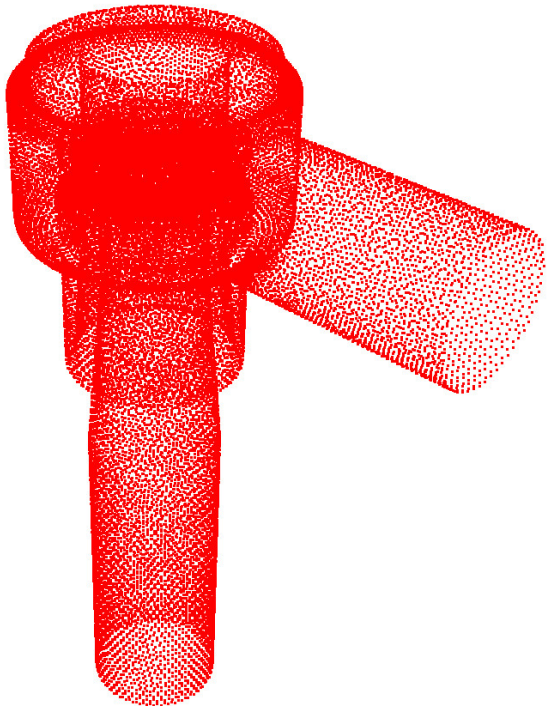

Fig. 6. Dipole pressure pulsation sound source information.

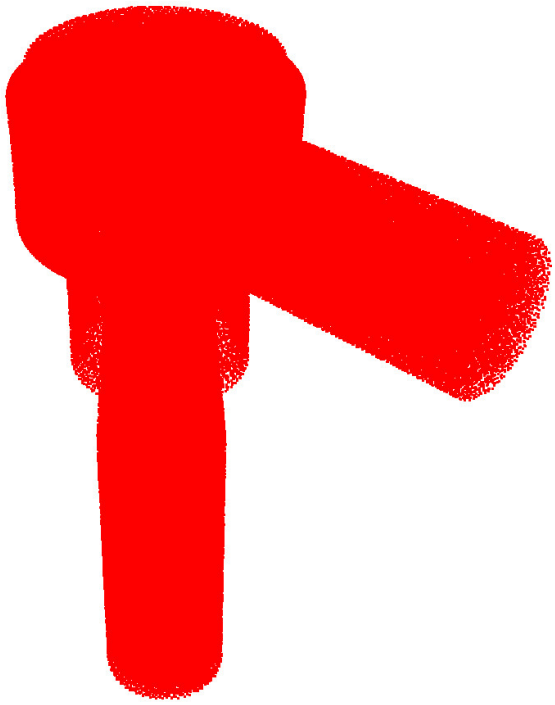

Fig. 7. Quadrupole velocity pulsation sound source information.

the Lighthill stress tensor based on the frequency domain. The dipole pressure fluctuation cloud map is obtained, as

shown in Figure 8. The contours of quadrupole velocity fluctuation are shown in Figure 9.

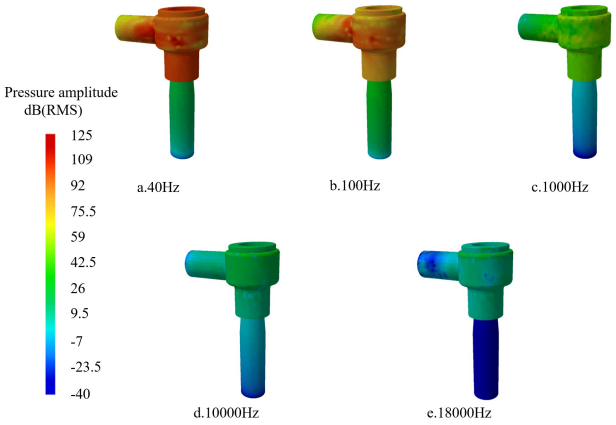

Fig. 8. Dipole pressure fluctuation program of the flow field at different frequencies.

From figure 8, it can be seen that the fluid medium has obvious pressure pulsation in the wide frequency band of 20 Hz to 18000Hz, which is distributed near the inner leakage hole and has a large amplitude fluctuation, showing the pulsation characteristics of the fluid medium and valve body structure wall coupling. The closer to the inner leakage hole, the greater the flow rate, and the stronger the pulsation characteristics of the coupling surface.

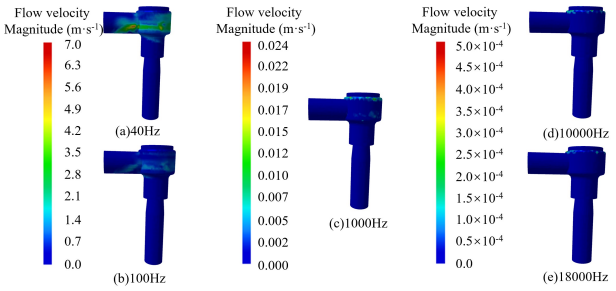

Fig. 9. The contours of quadrupole velocity fluctuation in the flow field at different frequencies.

From Fig. 9, it can be seen that the fluid velocity range is larger. The speed difference between 40Hz and 18kHz is several orders of magnitude. The velocity pulsation is mainly distributed near the internal leakage throttling region. Due to the existence of a boundary layer, the larger the Mach number is, the larger the normal velocity gradient of fluid flow direction is, and the more intense the velocity fluctuation in the local area is. The difference in velocity fluctuation amplitude at different frequencies can also reflect the distribution of leakage energy in the medium.

4.3. Boundary element mesh model and acoustic boundary condition

Different from structural finite element mesh, the precision of acoustic mesh is directly related to the highest computational frequency. The grid element is required to be less than 1/6 of the wavelength of the highest frequency calculation point. Considering the calculation range of 20 Hz 20000 Hz and the calculation accuracy requirement, the grid element length is 5.6 mm. The acoustic finite element mesh model of the safety valve is shown in Fig. 9. The sound pressure monitoring point 1 was set at the outlet of the safety valve Meanwhile, to ensure the accuracy of aerodynamic noise simulation of the safety valve and shield the influence of inlet and outlet pipeline noise, the outlet is defined as AML without reflection boundary property, and the acoustic impedance $Z_P = \rho_0 c_0$ of outlet fluid medium is set to 13.0×10^6 kg/m$^2 \cdot$ s.

5. Analysis of numerical simulation results of acoustic response

The acoustic response results of a certain frequency band are obtained using dipole, quadrupole, dipole, and quadrupole source information as excitation sources, respectively, as shown in Figs. 10, 11, and 12. The sound pressure spectrum curves of different acoustic responses at monitoring point 1 (Fig. 13) are shown in Fig. 14. Figure 14 shows that the sound pressure distribution excited by dipoles and quadrupoles is consistent with that excited by quadrupoles alone, which is different from that excited by dipoles alone. The results are consistent with the results of flow field analysis. When the safety valve leaks, the noise source is dominated by the quadrupole sound source generated by the jet and accompanied by the dipole sound source generated by the fluid-solid coupling.

6. Influence of different parameters on aeroacoustic field

6.1. Influence of inlet pressure on aerodynamic sound field

Under the action of a large pressure difference before and after the leakage hole in the safety valve, the fluid forms a series of turbulent vortexes along the axial direction downstream of the leakage hole.

Considering that the blocking jet noise will directly affect the sound pressure value of the aerodynamic sound field, the working condition with an inlet/outlet pressure ratio of less than 1.893 is set for study. To facilitate the simulation and comparative analysis under different parameters, the internal leakage gap of the safety valve is

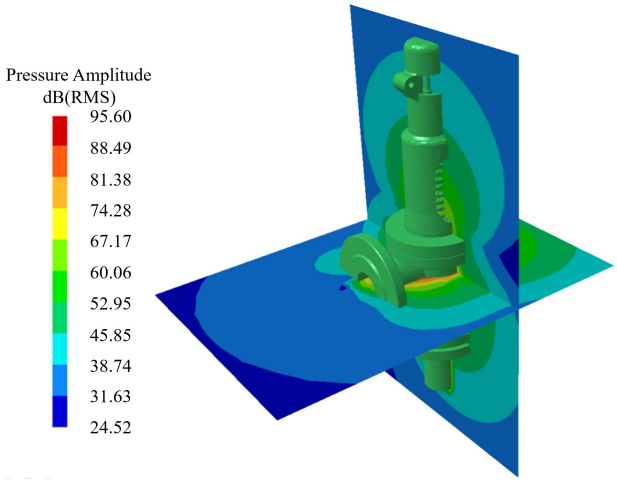

Fig. 10. Acoustic response 1 of safety valve at 70Hz Sound pressure distribution.

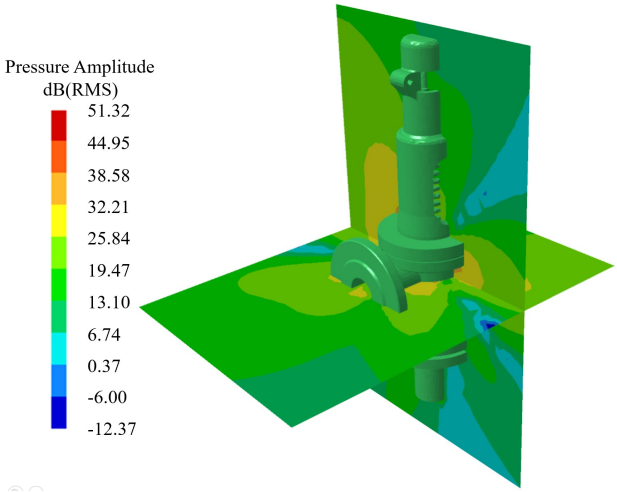

Fig. 11. Acoustic Response 2 of safety valve at 3770Hz sound pressure distribution.

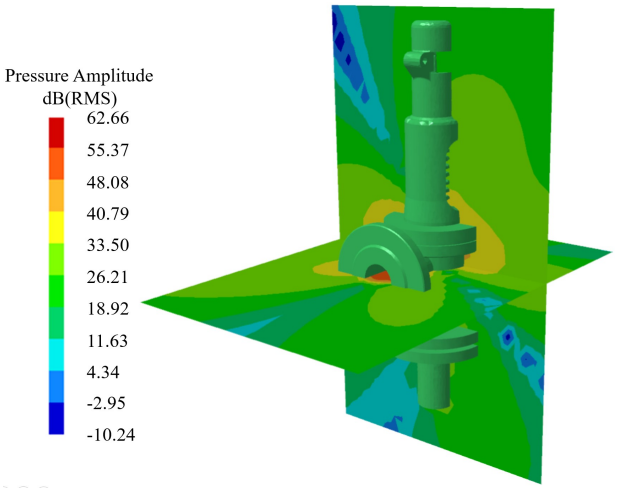

Fig. 12. Acoustic Response 3 of safety valve at 2520Hz sound pressure distribution.

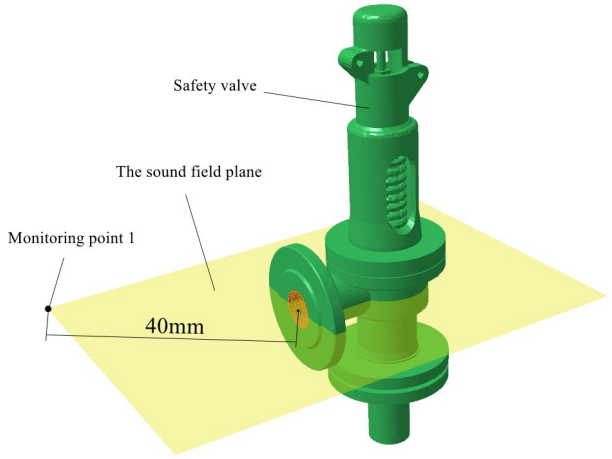

Fig. 13. Diagram of sound pressure Monitoring Point 1.

simplified by the equivalent diameter of the same round hole. The opening hole is 1 mm and the opening form is a round hole. The influence of inlet pressure on aerodynamic noise is analyzed, which are 0.11 MPa, 0.13 MPa, 0.15 MPa, and 0.17 MPa, respectively. The sound pressure-frequency characteristic curve of figure 10 is obtained.

Fig. 15 shows the sound pressure spectrum of the same measuring point of the safety valve in the same frequency range under different inlet pressures. It can be seen that the sound pressure spectrum curves under different pressures are similarly distributed. The peak sound pressure appears before 70 Hz, and the change of sound pressure level tends to be flat after 5KHz. With the increase of import pressure, the sound pressure level also increases. The internal leakage noise of the safety valve is mainly caused by the pressure pulsation dipole mainly based on the coupling force gradient between the moving fluid and the valve inner wall and the velocity pulsation quadrupole mainly based on the viscous shear stress in the jet section. With the change in pressure, the medium flow rate also changes. Therefore, the proportion of dipole and quadrupole in the total sound pressure level is not constant. The greater the inlet pressure is, the greater the medium flow rate is, and the greater the sound pressure level excited by the quadrupole sound source is. With the increase of inlet pressure, the flow velocity of the medium becomes faster, but the coupling surface between the medium and structural wall does not increase. Although the dipole sound source is also increasing, the increase is small. Therefore, the weighted sound pressure spectrum under different pressures cannot show the same regularity.

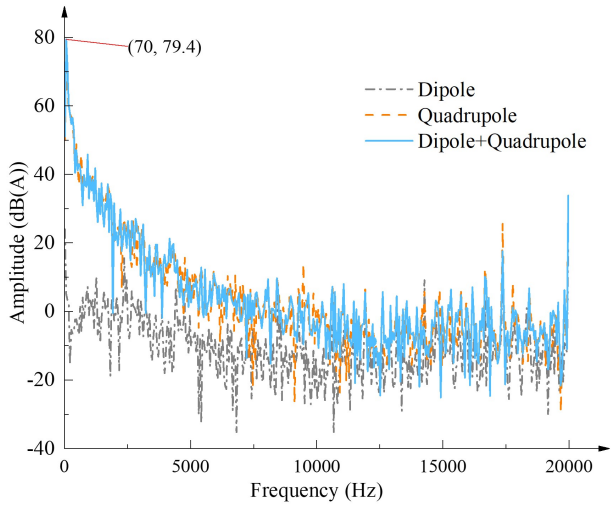

Fig. 14. Sound Pressure Spectrum of Different Acoustic Responses at Monitoring Point 1.

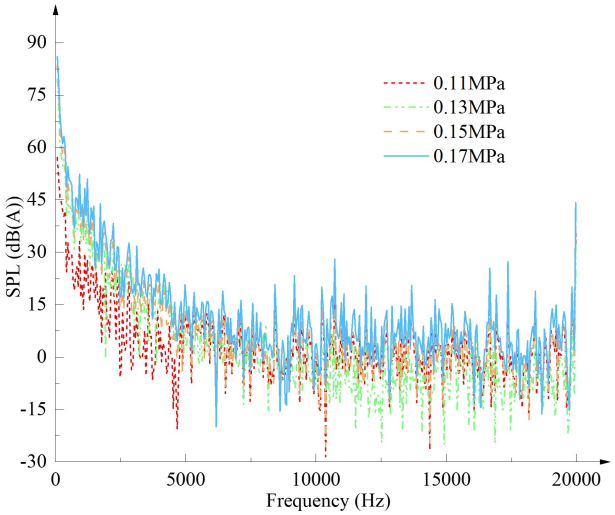

Fig. 15. Sound pressure spectrum under different inlet pressures.

As shown in table 2, the total sound pressure level of internal leakage noise in the frequency range of 20Hz 20KHz is obtained by weighting the calculated full frequency sound pressure value of internal leakage noise under different inlet pressures.

Table 2. Total SPL of internal leakage noise at the same monitoring point under different inlet pressures.

Inlet pressure (MPa)	0.11	0.13	0.15	0.17
Total SPL (dB)	60.42	80.24	87.51	89.32

Under the same hole and opening form, the sound pressure level of the internal leakage of the safety valve has a certain continuity with the change of pressure, which is characterized by linear characteristics. The continuity relationship between the inlet pressure and the total sound pressure level can be obtained, as shown in Figure 16.

In the case of other parameters unchanged, with the increase of pressure, the total sound pressure level of safety valve leakage increases. When the pressure ratio is close to 1.893, due to the phenomenon of blocking flow in the process of internal leakage, the internal leakage rate of the medium at the internal flow gap does not change, which inhibits the continued enhancement of the quadrupole sound source, and the dipole sound source increases with the increase of pressure, increasing the total sound pressure level.

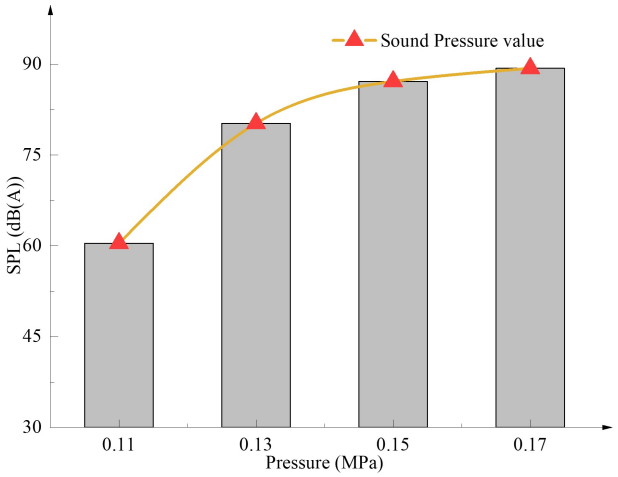

Fig. 16. Sound pressure level of safety valve under different inlet pressure.

6.2. Influence of Internal Leakage Hole Diameter on Aerodynamic Sound Field

To study the influence of internal leakage hole on aerodynamic noise, keeping the inlet pressure at 0.13 MPa, the internal leakage aerodynamic noise of the safety valve with an opening radius of 0.5 mm, 0.75 mm, 1 mm, 1.25 mm, and 1.5 mm was analyzed. The analysis results of the same monitoring point are processed by data information, and the frequency characteristic curve of the sound source is shown in Fig. 17.

As shown in Figure 18, different holes have obvious effects on the sound pressure level of the noise. the medium throttling is serious and the sound pressure level is small when the hole is small. When the hole is 0.75mm, there are peaks at 70Hz, 2KHz, 17.5KHz, and the peak value at 70Hz is 64.53dB. When the holes are 1 mm and 1.25 mm, the sound pressure level increases significantly and fluctuates stably; and the difference between the two is not very

Table 3. Total SPL of internal leakage noise at the same monitoring point under different inlet pressures.

Internal leakage diameter (mm)	0.5	0.75	1	1.25	1.5
Total SPL (dB)	51.03	65.02	80.24	86.94	73.12

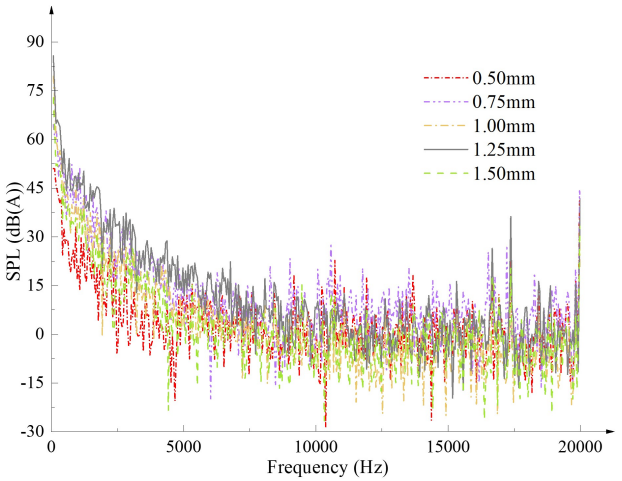

Fig. 17. Sound pressure spectrum under different hole dimension.

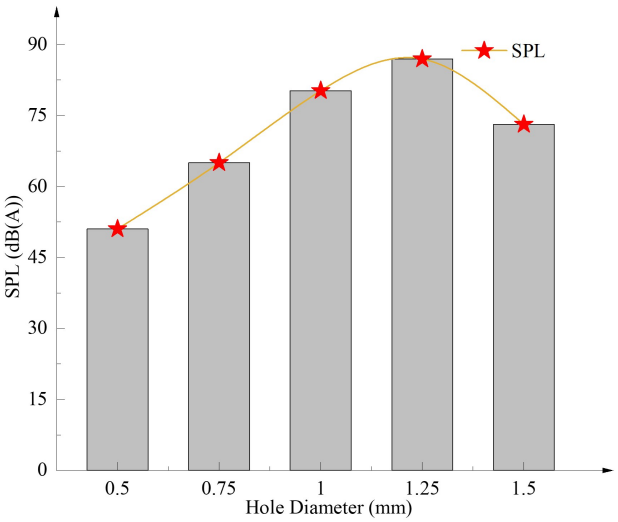

Fig. 18. Variation curve of sound pressure level with internal leakage diameter.

obvious, the amplitude of sound pressure enhancement is reduced; when the hole is1.5mm, the overall sound pressure level spectrum shows a decreasing trend. Compared with 1.25mm, the sound pressure level in20Hz-20KHz band shows a significant decrease.

The total sound pressure level of the leakage noise in the frequency range of 20Hz 20KHz is obtained by weighting the full frequency sound pressure value calculated by the leakage noise of the safety valve under different inlet pressures, as shown in table 3.

Under the same inlet pressure and opening form, the sound pressure level of internal leakage of the safety valve has quadratic linear characteristics with the change of internal leakage hole, and the relationship between different internal leakage holes and total sound pressure level is obtained, as shown in Fig. 18. As shown in Figure 18, the total sound pressure level is not a simple linear increase when the internal leakage hole of the safety valve increases gradually, which increases and then decreases, and decreases at the hole of 1.25 mm, and decreases to 86.94 dB at 1.5 mm. Although the internal leakage flow area increases, the Mach number decreases, and the internal viscous shear stress in the fluid medium decreases accordingly, resulting in a significant decrease in the velocity pulsation dominated by quadrupoles, and large flow cannot completely compensate for the weakening of the internal velocity pulsation. At the same time, as the hole increases, the coupling surface between the fluid medium and the structural wall also increases. However, due to the constant pressure before and after and the increasing flow resistance, the dipole pressure pulsation increases the proportion of the total sound pressure level, but it cannot make up for the decrease in the total sound pressure level. Therefore, the larger the internal leakage gap is, the flow sound pressure level generally increases first and then decreases, which is not unlimited.

7. Conclusion

The acoustic characteristics of the internal leakage noise of the safety valve and the relationship between the internal leakage hole and the medium pressure in the safety valve and the sound pressure level are studied. The following conclusions are drawn :

1. The flow field analysis shows that the noise source during internal leakage is mainly caused by a series of vortexes generated by the orifice jet, accompanied by the flow sound source generated by the coupling of fluid and wall. Based on the acoustic analysis, it can be seen that in the low-frequency range, the quadrupole sound source dominates. In the high-frequency range, the noise generated by the quadrupole sound source is close to the noise sound pressure level generated by the dipole sound source.

2. When the internal leakage diameter is the same, the

internal leakage noise is positively correlated with the medium pressure in the safety valve, and the changing trend of sound pressure level becomes slower with the increase of medium pressure.

3. When the pressure difference before and after the valve is consistent, the relationship between the internal leakage noise of the safety valve and the internal leakage diameter is a quadratic function. The internal leakage noise of the safety valve increases first and then decreases with the increase of the internal leakage diameter.

Acknowledgments

The study presented in this paper was supported by a program for the National Natural Science Foundation of China (Research Project: 51569012),the Double First-Class Key Program of Gansu Provincial Department of Education, and Gansu Province Science and Technology Program Funding: Grant No. 22CX8GA125.

References

[1] P.-S. Murvay and I. Silea, (2012) *"A survey on gas leak detection and localization techniques"* **Journal of Loss Prevention in the Process Industries *25***(6): 966–973. DOI: 10.1016/j.jlp.2012.05.010.

[2] I. van Kamp and F. van den Berg, (2018) *"Health effects related to wind turbine sound, including low-frequency sound and infrasound"* **Acoustics Australia *46***(1): 31–57. DOI: 10.1007/s40857-017-0115-6.

[3] M. M. Hotkani, M. R. M. Esmaeilpoor, M. Khadem, A. A. Garmaroudi, and K. Inanloorahatloo, (2022) *"Intermittent white noise exposure is associated with rat cochleae damage and changes in the gene expression"* **Egyptian Journal of Medical Human Genetics *23***(1): 104. DOI: 10.1186/s43042-022-00317-6.

[4] J. Ke, J. Du, and X. Luo, (2021) *"The effect of noise content and level on cognitive performance measured by electroencephalography (EEG)"* **Automation in Construction *130***: 103836. DOI: 10.1016/j.autcon.2021.103836.

[5] H. K. Yoon and K. P. Rhee, (2003) *"Identification of hydrodynamic coefficients in ship maneuvering equations of motion by estimation-before-modeling technique"* **Ocean Engineering *30***(18): 2379–2404. DOI: 10.1016/S0029-8018(03)00106-9.

[6] J. Taghinia, M. M. Rahman, and T. Siikonen, (2015) *"Large eddy simulation of a high-pressure homogenizer valve"* **Chemical Engineering Science *131***: 41–48. DOI: 10.1016/j.ces.2015.03.041.

[7] B. Chen, Y. Lu, W. Li, X. Dai, X. Hua, J. Xu, Z. Wang, C. Zhang, D. Gao, Y. Li, et al., (2022) *"DPM-LES investigation on flow field dynamic and acoustic characteristics of a twin-fluid nozzle by multi-field coupling method"* **International Journal of Heat and Mass Transfer *192***: 122927. DOI: 10.1016/j.ijheatmasstransfer.2022.122927.

[8] Y. Ren, Z. Wu, X. Meng, G. Ou, J. Kou, H. Jin, and L. Guo, (2022) *"Large eddy simulation of water jets under transcritical and supercritical conditions"* **The Journal of Supercritical Fluids *187***: 105648. DOI: 10.1016/j.supflu.2022.105648.

[9] Y.-M. Li, B.-K. Li, F.-S. Qi, and X.-C. Wang, (2017) *"Numerical investigation of the interaction of the turbulent dual-jet and acoustic propagation"* **Chinese Physics B *26***(2): 024701. DOI: 10.1088/1674-1056/26/2/024701.

[10] F. Liao, (2022) *"On turbulent flow and aerodynamic noise of generic side-view mirror with cell-centred finite difference method"* **Journal of Turbulence *23***(3): 97–123. DOI: 10.1080/14685248.2022.2037621.

[11] S. Hambric, D. Boger, J. Fahnline, and R. Campbell, (2010) *"Structure-and fluid-borne acoustic power sources induced by turbulent flow in 90 piping elbows"* **Journal of Fluids and Structures *26***(1): 121–147. DOI: 10.1016/j.jfluidstructs.2009.10.001.

[12] T. Zhang, Y. Zhang, and H. Ouyang, (2015) *"Structural vibration and fluid-borne noise induced by turbulent flow through a 90 piping elbow with/without a guide vane"* **International Journal of Pressure Vessels and Piping *125***: 66–77. DOI: 10.1016/j.ijpvp.2014.09.004.

[13] K.-X. Ren, Z.-J. Shuai, X. Wang, J. Jian, T. Yu, L.-Y. Dong, W.-Y. Li, and C.-X. Jiang, (2022) *"Aerodynamic noise prediction of a high-speed centrifugal fan considering impeller-eccentric effect"* **Engineering Applications of Computational Fluid Mechanics *16***(1): 780–803. DOI: 10.1080/19942060.2022.2042392.

[14] C. Zhong, L. Hu, J. Gong, C. Wu, S. Wang, and X. Zhu, (2021) *"Effects analysis on aerodynamic noise reduction of centrifugal compressor used for gasoline engine"* **Applied Acoustics *180***: 108104. DOI: 10.1016/j.apacoust.2021.108104.

[15] X.-F. Niu, Y. Li, and X.-N. Wang, (2021) *"Numerical study of aerodynamic noise behaviors for a vertically-installed flat strut behind an asymmetrical airfoil"* **European Journal of Mechanics-B/Fluids *88***: 17–33. DOI: 10.1016/j.euromechflu.2021.02.004.

[16] J. Zhang, Z. Lian, Z. Zhou, M. Xiong, M. Lian, and J. Zheng, (2021) *"Acoustic method of high-pressure natural gas pipelines leakage detection: Numerical and applications"* **International Journal of Pressure Vessels and Piping *194***: 104540. DOI: 10.1016/j.ijpvp.2021.104540.

[17] H. Liu, R. Zhou, Q. Pan, L. Dong, Q. Ma, Z. Cheng, and X. Wang, (2022) *"Noise spectrum characteristics of marine pump units induced by different excitation sources"* **Scientific Reports *12***(1): 8678. DOI: 10.1038/s41598-022-12755-8.

[18] J.-y. Qian, L. Wei, G.-r. Zhu, F.-q. Chen, and Z.-j. Jin, (2016) *"Transmission loss analysis of thick perforated plates for valve contained pipelines"* **Energy Conversion and Management *109***: 86–93. DOI: 10.1016/j.enconman.2015.11.058.

[19] H. Wang, Z. Lai, D. Wu, K. Zhang, and M. Zheng, (2022) *"Investigation of the friction-induced vibration of a novel four-way reversing valve using spectral kurtosis and number of peaks spectrum"* **Mechanical Systems and Signal Processing *166***: 108425. DOI: 10.1016/j.ymssp.2021.108425.

[20] S. Li, J. Hou, W. Pan, Z. Wang, and Y. Kang, (2020) *"Study on aerodynamic noise numerical simulation and characteristics of safety valve based on dipole and quadrupole"* **Acoustics Australia *48***: 441–454. DOI: 10.1007/s40857-020-00201-6.